Thymus serpyllum L. (wild thyme) plant as a promising native biosorbent for the adsorption of Cu(II) and Pb(II) ions

Mária Kováčová
Ústav geotechniky SAV: Ustav geotechniky Slovenskej akademie vied
Halyna Yankovych
Ústav geotechniky SAV: Ustav geotechniky Slovenskej akademie vied
Mariano Casas Luna
VUT: Vysoke uceni technicke v Brne
Michaela Remešová
VUT: Vysoke uceni technicke v Brne
Lenka Findoráková
Ústav geotechniky SAV: Ustav geotechniky Slovenskej akademie vied
Martin Stahorský
Ústav geotechniky SAV: Ustav geotechniky Slovenskej akademie vied
Ladislav Čelko
VUT: Vysoke uceni technicke v Brne
Matej Baláž (balazm@saske.sk)
Ústav geotechniky SAV: Ustav geotechniky Slovenskej akademie vied https://orcid.org/0000-0001-6563-7588

Research Article

Keywords: Biosorption, lead, copper, Thymus serpyllum L. plant

Posted Date: April 22nd, 2022

DOI: https://doi.org/10.21203/rs.3.rs-1524327/v1

Abstract

The presented study proposes a new potential biosorbent- *Thymus serpyllum* L. (wild thyme) plant, which showed to be highly efficient in rapid adsorption of Cu(II) and Pb(II) ions with higher adsorption capacity towards Pb(II) ions. Apart from biochars, that are commonly used for adsorption, here we report the direct use of native plant. The influence of different parameters (pH, contact time, adsorbent dosage) on the adsorption process as well as the adsorption in a binary system of selected metal contaminants was examined. The highest adsorption capacity for Cu(II) ions (q_e = 12.66 mg g^{-1}) was achieved after 10 minutes of adsorption at 16 g L^{-1} adsorbent dosage at natural pH. The highest obtained adsorption capacity for Pb(II) ions was 53.13 mg g^{-1} after 30 minutes at 12 g L^{-1} adsorbent dosage at unadjusted pH. The combination of characterization methods (SEM/EDX, TGA, FT-IR, XPS and ζ-potential measurements) were applied to estimate the removal mechanism during the adsorption of Cu(II) and Pb(II) ions on the plant biosorbent surface. The characteristic shifts were observed in the thermogravimetric curves and FT-IR spectra and together with the changes of pH during adsorption process confirmed the combined adsorption mechanism consisting of the ion exchange at the lower Cu(II) and Pb(II) concentrations and the complexation and chelation at higher contaminants' concentrations.

1. Introduction

The contamination of drinking water and wastewaters by heavy metal ions is a very important environmental issue as the intoxication with those substances can cause various health problems with the central and peripheral nervous system, gastrointestinal, cardiovascular, hematopoietic and renal systems being the most susceptible to damage (Ibrahim et al. 2006). Copper and lead belong to the most common heavy metal contaminants (Mudhoo et al. 2012). Lead is a good example of a typical heavy metal with a number of harmful effects when accumulated in the human body even at low concentrations (Wan et al. 2010). The principal targets for lead toxicity are the central and peripheral nervous systems, but bones and kidney are affected as well (Mudhoo et al. 2012). Moreover, lead inhibits the biosynthesis of haem and accelerates the destruction of erythrocytes which causes anaemia (Moore 1988). Copper is generally considered less harmful than lead, although the Cu(II) ions represent the most toxic form of copper for aquatic species (Adriano 2001). The presence of Cu(II) ions in drinking water can cause diarrhoea, vomiting, abdominal pain, nausea, chronic disorders and kidney damage (Awual et al. 2013). When ingested at high concentrations, copper promotes oxidation and may be a risk factor for cancer (Schmuhl et al. 2001). Cu(II) ions are extremely dangerous for people with Wilson disease, which is a genetic disorder that causes the accumulation of copper in different tissues and if left untreated, it may damage the liver, central nervous system and in the worst case cause death (Guerrero-Jimenez et al. 2019). According to the DIRECTIVE (EU) 2020/2184, the maximum allowed concentration in water intended for human consumption for Cu(II) ions is 2.0 mg L^{-1}. In relation to Pb(II) ions, the parametric value of 5 µg L^{-1} shall be met, at the latest, by 12 January 2036. The parametric value for lead until that date shall be 10 µg L^{-1} (European Parliament and Council of the European Union 2020).

Among the many available methods for water remediation (e.g. reverse osmosis, ion exchange, electrodialysis, ultrafiltration), the process of adsorption and specifically biosorption has an inevitable place and seems to be preferable because of low operation costs (Czikkely et al. 2018; Beni and Esmaeili 2020). The search for sustainable materials as adsorbents is one of the most developing areas of research these days. Natural-based materials such as bacteria, algae, fungi, plants, biopolymers, the skin of animals and fruits, or even natural waste materials have attracted increasing attention as biosorbents for heavy metals owing to their renewable, biodegradable and environmentally friendly properties (Duan et al. 2013; Chen et al. 2017; Baláž 2021).

Biosorbents derived from plants include a wide range of materials such as visible parts of plants (shoots, bark and foliage) (Sert et al. 2008; Reddy et al. 2011), roots and seasonal parts (blossom, fruit, seeds, stones, cones, hulls, husks etc.) (Elangovan et al. 2008; Oliveira et al. 2008; Witek-Krowiak et al. 2011). Plant-derived materials consist of biopolymers, mostly various forms of lignocellulose (lignin, cellulose, hemicellulose, etc.) and tannins that contain specific functional groups in their structure (e.g. hydroxyl, carboxyl, carbonyl, thiol, amine and others) allowing binding of chemical compounds. The mechanism of biosorption is very complex and consists of a number of physical and chemical processes such as adsorption (physical, chemisorption), ion exchange, complexation or microprecipitation. Each biosorbent has its own characteristics such as a chemical structure or porosity that affects its sorption capacity and reactivity under given conditions. The physical and chemical parameters (pH, temperature, biosorbent dosage, etc.) also influence the effectiveness of biosorption (Witek-Krowiak 2012).

When selecting the appropriate plant for biosorption, the most common ones are the best choice. *Thymus serpyllum* L. (wild thyme) is an aromatic flowering plant belonging to the *Lamiaceae* family, which is widely used for medicinal as well as food seasoning purposes. *Thymus serpyllum* L. contains high levels of essential oils and polyphenolic compounds, which are either phenolic acids (e.g. chlorogenic, caffeic and rosmarinic acids) or flavonoids (e.g. luteolin and apigenin glucuronide) that are responsible for high radical scavenger potential and anti-inflammatory properties (Jovanovic et al. 2017). This plant has already been used for the removal of antimony ions in (Littera et al. 2011) but more complex studies regarding the adsorption of more heavy metals or the discussion of the adsorption mechanism have not been published until now.

The aim of the presented paper was to investigate the adsorption of Cu(II) and Pb(II) ions on the native *Thymus serpyllum* L. (wild thyme) plant from the model solutions in detail, including the assessment of the adsorption mechanism by employing a combination of diverse characterization methods. Such a study has never been reported.

2. Materials And Methods

2.1. Materials

Thymus serpyllum L. (wild thyme) plant (SER) was purchased from a local company, Agrokarpaty, s.r.o., Slovakia, concerned with a cultivation of medicinal plants. The plant was milled in a kitchen mixer and sieved to reach the particle size ≤ 1 mm. Copper nitrate trihydrate $Cu(NO_3)_2.3H_2O$, lead nitrate $Pb(NO_3)_2$, cadmium nitrate tetrahydrate $Cd(NO_3)_2.4H_2O$, zinc nitrate hexahydrate $Zn(NO_3)_2.6H_2O$, iron nitrate nonahydrate $Fe(NO_3)_3.9H_2O$, aluminum chloride hexahydrate $AlCl_3.6H_2O$ and cobalt chloride hexahydrate $CoCl_2.6H_2O$ were used as chemicals without further purification for a preparation of model solutions. All chemicals were purchased from Merck KGaA, Germany, and ITES Vranov, s.r.o., Slovakia, and were of analytical grade.

2.2. Methods

X-ray diffraction (XRD) patterns of the samples after adsorption were obtained using a D8 Advance diffractometer (Bruker, Billerica, MA, USA) with CuKα radiation of 0.15407 nm wavelength at 40 kV accelerating voltage and 40 mA electric current. The samples were scanned over a 15°–70° range of diffraction angle (2θ).

The concentration of copper(II), lead(II), cadmium(II), zinc(II), iron(III), aluminium(III) and cobalt(II) ions in the initial and residual adsorption solutions as well as the concentration of calcium(II), magnesium(II), potassium(I) and sodium(I) in a filtrate after washing of pure SER plant were determined by atomic absorption spectrometry (AAS) using an atomic absorption spectrometer SPECTRAA L40/FS (Varian, Crawley, UK).

The morphology of the samples and elemental distribution were studied by the scanning electron microscope (SEM) Lyra3 (Tescan, Czech Republic) equipped with an energy-dispersive X-ray spectroscopy (EDX) unit X-Max 50 (Oxford Instruments, United Kingdom). The SEM/EDX examination was carried out in back-scattered electron (BSE) and secondary electron (SE) modes using an acceleration beam voltage of 10 keV. The EDX mapping spectra were analysed using AZtec software (Oxford Instruments NanoAnalysis, United Kingdom). Prior to SEM/EDX examination, each dry SER sample was placed on double-sided adhesive carbon tape and coated with a 20 nm thick carbon layer using a sputter coater Leica EM ACE600 (Leica Microsystems, Germany).

Simultaneous TG/DTG and DTA analysis of the studied compounds were carried out using STA 449 Jupiter thermal analyzer (Netzsch, Germany). A 30 mg of sample was placed in Al_2O_3 crucible and heated from 25°C up to 1300°C at linear heating rate 5°C min^{-1} in synthetic air (N_2 80%,O_2 20%) combined with argon atmosphere.

FT-IR spectra were recorded using a Tensor 29 infrared spectrometer (Bruker, Germany) using the ATR method in the range 4000–650 cm^{-1}.

The X-ray photoelectron spectroscopy (XPS) of the pure SER plant and after Cu and Pb adsorption was performed in XPS – Kratos Axis Supra apparatus (Manchester, UK) working with a monochromatic Al-Kα radiation at an emission current of 15 mA. Wide and high-resolution spectra were acquired with a pass

energy of 80 eV and 20 eV, respectively. The spectra were calibrated setting the C1s emission at 284.7eV. The deconvolution and fitting of the interested elements, i.e., Cu2p, Pb4f, C1s, and O1s, were carried out using the CasaXPS software (version 2.3.22) by applying a Spine-Shirley background and a Gaussian/Lorentzian (70/30) fitting for the individual high-resolution spectra peaks.

The zeta potential (ζ-potential) measurements were conducted using a Zetasizer Nano ZS (Malvern, UK). Prior to measurements, 20 mg of each sample was sonicated in 10 mL of 10 mM NaCl solution for 10 minutes. NaCl solution was used to maintain a minimum level of conductivity. ζ-potential values were obtained by applying the Smoluchowski equation built into the Malvern Zetasizer software. The measurements were repeated 3 times for each sample.

2.3. Adsorption studies

All adsorption experiments were performed at laboratory temperature in a batch mode in Erlenmeyer flasks on the orbital shaker.

Preliminary experiment. At first, the adsorption potential of SER plant was investigated in a model solution prepared from a corresponding mass of chemically pure $Cd(NO_3)_2.4H_2O$, $Zn(NO_3)_2.6H_2O$, $Cu(NO_3)_2.3H_2O$, $Pb(NO_3)_2$, $Fe(NO_3)_3.9H_2O$, $AlCl_3.6H_2O$ and $CoCl_2.6H_2O$ dissolved in distilled water to obtain the concentration 20 mg L^{-1} for each element in the final solution. Such a low concentration was selected because the 100% adsorption of metal ions from the solution was expected. The mass of adsorbent (SER sample) was 0.12 g, the volume of model solution was 0.06 L and the contact time was 2 hours. These conditions were applied according to the literature data (Kong et al. 2014).

Based on the preliminary experiment mentioned above, we chose Cu(II) and Pb(II) for the consecutive experiments to scrutinise the adsorption potential of SER. As a first step, we studied the adsorption of Cu(II) and Pb(II) at three different concentrations (c = 20, 200 and 1000 mg L^{-1}). Higher concentrations were chosen to investigate selective adsorption to study competitive adsorption. The adsorption was performed in the same way as had already been mentioned, but the contact time was 5, 10, 15, 30, 45, 60, 90 and 120 minutes. The mass of adsorbent was reduced to 0.06 g and the volume of copper/lead nitrate solution was 0.03 L, which means the adsorbent dosage remained unchanged.

Adsorbent dosage. Thereafter, the subsequent experiments were concerned with determining the optimal adsorption parameters. The experimental conditions were maintained as a mass of adsorbent 0.06 g and volume of copper/lead nitrate solution 0.03 L with concentration 200 mg L^{-1}. During the experiment for defining the best adsorbent dosage, the concentrations 0.4, 0.8, 1, 2, 3, 4, 8, 12, 16, 20 and 24 g L^{-1} were examined.

pH investigation. The dependence of the adsorption capacity on pH was analysed in the pH range from 1 to 5 for Cu(II) ions and from 1 to 6 for Pb(II) ions. The pH values of $Cu(NO_3)_2.3H_2O$ and $Pb(NO_3)_2$ solutions were adjusted by adding appropriate amount of 0.1 M NaOH or 0.1 M HNO_3 solutions.

Kinetic studies. To study the adsorption kinetics of Cu(II) and Pb(II) ions, SER sample with concentration 2 g L^{-1} (0.06 g in 0.03 L) and metal-containing model solutions with concentration 200 mg L^{-1} were stirred for 1, 3, 5, 7, 10, 15, 30 and 60 minutes. In order to find the optimal kinetic model for the studied process, the experimental data were fitted to Lagergren's pseudo-first (Lagergren 1898) and Ho's pseudo-second (Ho et al. 1996) order kinetic models.

Isotherms modelling. The adsorption isotherm investigations were performed in the concentration range 10–1000 mg L^{-1} at the optimal adsorption conditions determined by previous experiments for Cu(II) and Pb(II) ions, respectively. The adsorption isotherm data were processed by the linearised forms of equations for Langmuir and Freundlich isotherm models and the appropriate parameters were calculated (Freundlich 1906; Langmuir 1916; Yankovych et al. 2021).

Competitive adsorption. To investigate the influence of metal ions coexistence on the adsorption, the binary solution of both metals was prepared. The binary solution contained $Cu(NO_3)_2.3H_2O$ and $Pb(NO_3)_2$ with the concentration 200 mg L^{-1} for each heavy metal (to achieve competitiveness), the mass of adsorbent was 0.48 g, the volume of binary solution was 0.03 L, the agitation time was 30 minutes and pH was natural.

Estimation of the adsorption mechanism. In order to determine whether the ion exchange process is involved in the adsorption of Cu(II) and Pb(II) ions, we measured the content of alkali- Na(I), K(I) and alkaline earth- Ca(II), Mg(II) elements released into the aqueous solution from pure SER plant as described in (Martinez et al. 2006) and the total content of released cations was expressed in mEq g^{-1}. Afterwards, the adsorption of Cu(II) and Pb(II) ions on the SER biosorbent after washing and drying was performed under the optimal conditions identified by the previous experiments. Namely, for the adsorption of Cu(II) ions 0.48 g SER and 10 minutes contact time was used and for the adsorption of Pb(II) ions 0.36 g SER and 30 minutes contact time was applied. In both cases, the ionic concentration of 750 mg L^{-1} was used, as the maximum adsorption capacity for both target metals was reached at this point.

The adsorption capacity (or uptake) at equilibrium q_e or at time t q_t (mg g^{-1}) of the adsorbent and the removal percentage of the adsorbed heavy metals were calculated according to the Equations 1 and 2 described in (Zou et al. 2015; Cui et al. 2021):

$$q_{e/t} = \frac{\left(C_0 - C_{e/t}\right)V}{m}$$

1

$$R = \frac{C_o - C_t}{C_o} * 100\%$$

where C_0 (mg L^{-1}) is the initial concentration, C_e or C_t (mg L^{-1}) is the concentration in equilibrium or at time t, respectively, V (L) is the volume of the adsorbate solution and m (g) is the mass of the adsorbent.

3. Results And Discussion

3.1. Preliminary adsorption experiments

3.1.1. The experiment with model solution

According to the preliminary experiment with a model solution containing a combination of various ions (see Table S1 in the Supplementary information), *Thymus serpyllum* L. plant (SER) showed the best adsorption potential towards Fe(III), Cu(II) and Pb(II) ions as the concentration of these three ions decreased markedly in comparison with the other four tested ones. In agreement with the obtained results, we chose to focus on the adsorption of Cu(II) and Pb(II) in the following experiments. We did not study the adsorption of Fe(III) ions further because at pH > 4.0 Fe(III) ions precipitate in a form of $Fe(OH)_3$ and therefore very acidic conditions are required for their adsorption (Bhattacharyya and Sen Gupta 2006; Ucer et al. 2006) and some structures of the plant adsorbent would most probably decompose under such conditions. Moreover, Cu(II) and Pb(II) ions are more toxic and more dangerous in lower concentrations than Fe(III) ions.

3.1.2. Adsorption performance at different concentrations

The adsorption capacity values (q_t) for the adsorption of Cu(II) and Pb(II) ions at three different concentrations (c = 20, 200 and 1000 mg L^{-1}) showed the most consistent results at c = 200 mg L^{-1} (see Figure S1 and S2 in the Supplementary information), thus we worked with this concentration in the subsequent experiments.

3.2. Determination of the optimal adsorption parameters

3.2.1. The effect of pH

The pH is one of the most important parameters affecting the adsorption of metal ions because the surface charge of an adsorbent could be modified by changing the pH of the solution and partly due to the fact that hydrogen ions are strong competing sorbates (Cruz-Olivares et al. 2010). In order to discover the influence of this parameter on the adsorption of Cu(II) and Pb(II) ions, the metal solutions with different pH values ranging between 1 to 6 were prepared due to the precipitation of metals in a form of insoluble substances at higher pH values. At very acidic pH (1 and 2) the uptake of Cu(II) and Pb(II) ions was very low and with increasing pH, uptake for both ions raised (Fig. 1a). The best results for Cu(II) ions were achieved at pH = 4 and for Pb(II) ions, the uptake in the pH range from 4–6 was approximately the same. Considering that the natural pH of both nitrate solutions was in the optimal pH range, we

continued with following experiments at natural pH. The study by Littera et al. (Littera et al. 2011) concerned with the adsorption of Sb(III) ions on the same plant revealed that the Sb(III) removal was the highest in the pH range 3.3–4.6, however the authors selected pH 5.6 for further experiments.

3.2.2. The effect of contact time

To study the appropriate contact time for the adsorption of Cu(II) and Pb(II) ions, the kinetic experiments were performed (Fig. 1b). The initial uptake after the first minute was quite high for both ions (q_t = 8.5 mg g^{-1} and 34.7 mg g^{-1} for Cu(II) and Pb(II) ions, respectively) and later slowed down which was more prominent in case of Cu(II) adsorption. The uptake for Cu(II) ions was pretty constant after 10 minutes (q_t = 11 mg g^{-1}) and in the case of Pb(II) ions after 30 minutes (q_t = 49.4 mg g^{-1}), therefore these contact times were selected in further experiments.

3.2.3. The effect of adsorbent dosage

The dosage of adsorbent is another important parameter affecting the adsorption ability of the studied biosorbent. The Fig. 1c displays that we examined 11 different SER concentrations (starting from 0.4 g L^{-1} up to 24 g L^{-1}) in our experiments. The removal rate for both heavy metal ions raised gradually and the plateau was reached at 16 g L^{-1} with 55.7% removal for Cu(II) ions and at 12 g L^{-1} with 86.1% removal for Pb(II) ions. Further increase in the adsorbent dosage did not result in higher removal of the studied pollutants. The adsorbent dosage 16 g L^{-1} was found to be optimal for adsorption of Sb(III) ions when using the same plant in the paper by Littera et al. (Littera et al. 2011).

3.2.4. The binary system adsorption

To explore the combined adsorption onto SER biosorbent, the adsorption experiment with a binary metal system containing both Cu(II) and Pb(II) ions was performed. The results presented in Fig. 1d showed that the removal efficiency was higher for Pb(II) ions and was not affected by the presence of both metal ions in the solution as the removal 61.5% and 90.1% for Cu(II) and Pb(II) ions, respectively, was very similar to the results presented in Fig. 1c thus suggesting that different functional groups are involved in the adsorption process of these two ions.

3.3. Adsorption kinetics

In order to analyze the adsorption kinetics of the studied metals, pseudo-first and pseudo-second order equations were applied and the obtained kinetic parameters are summarised in Table 1. According to these results, the adsorption of Cu(II) and Pb(II) ions follows the pseudo-second-order model as the correlation coefficients are close to 1 (R^2 = 0.9997 and 0.9961, respectively). Littera et al. (Littera et al. 2011) also achieved higher correlation coefficient for the pseudo-second-order model during the adsorption of Sb(III) ions. This suggests that the chemisorption of Cu(II) and Pb(II) ions is the rate-determining step of the adsorption process and involves the chemical interaction such as ion exchange or chelation between Cu(II) and Pb(II) ions and polar functional groups on the adsorbent surface (Huang

et al. 2016). The better fit of the pseudo-second-order model also indicates the existence of two types of active adsorption sites on the adsorbent surface (Yankovych et al. 2021).

Table 1
Kinetic parameters for adsorption of Cu(II) and Pb(II) ions onto *Thymus serpyllum* plant

Metals	Pseudo-first order			Pseudo-second order			
	$\ln(q_e-q_t) = \ln q_e - k_1 t$			$t/q_t = 1/(k_2 q_e^2) + t/q_e$			
	k_1	$q_{e, cal}$	R^2	k_2	$q_{e, cal}$	R^2	$q_{e, exp}$
Cu(II)	0.0016	1.87	0.0051	0.29575	21.98	0.9997	12.66
Pb(II)	-0.0464	16.61	0.9172	0.00893	50.51	0.9961	53.13

Notes: $q_{e, cal}$, $q_{e, exp}$ (mg g^{-1}) the calculated and the experimental adsorption capacity at equilibrium time, respectively, q_t (mg g^{-1}) the adsorption capacity at time t, k_1 (min^{-1}) and k_2 (g mg^{-1} min^{-1}) the kinetic rate constants of the pseudo-first-order and pseudo-second order models, respectively, R^2 correlation coefficient

3.4. Adsorption isotherms

The main adsorption characteristics were analysed by fitting the experimental results of adsorption isotherms (Fig. 2) using two mostly used models (Langmuir and Freundlich isotherm model) and the obtained parameters are summarised in Table 2. The Langmuir equation is valid for the monolayer adsorption onto a surface of the adsorbent with a finite number of identical sites (Huang et al. 2007). In our case, the Langmuir model suited better for the adsorption of Cu(II) ions, which implied that the adsorption of Cu(II) was limited to one molecular layer and the maximum monolayer adsorption capacity- Q_m was calculated to be 14.64 mg g^{-1}. This model was also found to be suitable for the adsorption of Sb(II) ions in (Littera et al. 2011), and the observed adsorption capacity therein was 8.77 mg g^{-1}. In the case of Pb(II) ions adsorption in our study, the value of correlation coefficient was higher for Freundlich isotherm model which suggests that the adsorption occurred on the heterogeneous surface of the adsorbent. The favourability and capacity of the adsorbent/adsorbate system are related to the magnitude of 1/n and the higher fractional values of 1/n suggest that the system has strong adsorption forces (Liu et al. 2019a).

Table 2
Adsorption isotherms parameters for Cu(II) and Pb(II) ions adsorption on *Thymus serpyllum* plant

Metals	Langmuir model				Freundlich model			
	$C_e/q_e = 1/(K_L*Q_m) + C_e/Q_m$				$\ln q_e = \ln K_F + (1/n) * \ln C_e$			
	K_L	Q_m	$q_{e\,exp}$	R^2	K_F	1/n	n	R^2
Cu(II)	$7.3*10^{-3}$	14.64	12.66	0.98	8.07	0.81	1.23	0.91
Pb(II)	$1.82*10^{-2}$	27.40	53.13	0.86	3.79	1.14	0.88	0.98

Notes: K_L (L mg^{-1}) the Langmuir adsorption equilibrium constant, Q_m (mg g^{-1}) the maximum monolayer adsorption capacity, $q_{e,\,exp}$ (mg g^{-1}) the experimental adsorption capacity at equilibrium time R^2 correlation coeficient, K_F (L g^{-1}) the Freundlich constant indicating the adsorption capacity, **n** (g L^{-1}) the Freundlich constant representing the adsorption intensity

According to (Bayo 2012) the difference in selectivity and adsorption capacity of Cu(II) and Pb(II) ions onto an adsorbent can be associated with the physicochemical properties of these two ions such as the differences in ionic radius, electronegativity, hydrated radius and atomic weight.

3.5. Possible mechanism of Cu(II) and Pb(II) ions adsorption onto *Thymus serpyllum* L.

The investigation of adsorption mechanism is a very important issue with the potential to predict and control the adsorption process. Therefore, the available advanced methods like SEM/EDX, TGA, FT-IR, XPS and ζ-potential measurements were utilized to estimate the removal mechanism during the adsorption of Cu(II) and Pb(II) ions on the SER surface. Previous studies have revealed that the elimination of these contaminants can be realised by different processes, among which the complexation with surface carboxylic groups, the chelation with nitrogen moieties with formation of a coordinate bond between the lone pair of nitrogen and d-orbitals of heavy metals and the ion exchange are the most common (Mahaninia et al. 2015; Forgionny et al. 2021; Xu et al. 2021).

In order to prove the adsorption process as well as to estimate the distribution of the adsorbed ions on the biosorbent surface, the SEM/EDX observations were done. As illustrated in Fig. 3, the adsorbed Cu(II) and Pb(II) ions are evenly distributed on the SER surface in the form of precipitates, as small spheres and particles with indefinite shape for Cu and Pb adsorption, respectively (Fig. 3c and f). The EDS mapping has shown the inhomogeneous distribution of Cu and Pb elements (Fig. 3b and e). The amount of lead in the selected region in Fig. 3e is much higher than that of Cu in Fig. 3b.

To determine the nature of the precipitates, the XRD measurements of the metal-laden adsorbents were performed. However, no crystalline phases could be identified on the diffractograms (see Figure S3 in

Supplementary information). Hence, it can be suggested that the available amount of crystalline phase cannot be detected because of the interfering effect of the plant matrix (this might be the reason in the case of Cu(II) ions adsorption) or because the precipitates most probably have an amorphous nature (this might be the case of Pb(II) ions adsorption).

To better understand the processes present during the adsorption of Cu(II) and Pb(II) ions on SER surface, the thermogravimetric analysis of the samples was performed. Figure 4 represents the thermogravimetric curves of TG-DTG/DTA analysis of the samples. As can be seen from the Fig. 4a, there are three exothermic peaks at 90°C, 324°C and 480°C on the thermogram of native SER plant. The mass loss at 90°C includes the loss of moisture present in the sample (~ 10.6 wt.%). Next, the fast weight losses at 324°C (~ 53.1 wt.%). and 480°C (~ 33.5 wt.%). were detected. These two processes can be considered as the decomposition of the chemical groups on the SER surface. According to (Shafeeyan et al. 2010), the first exothermic peak can be related to the decomposition of the carboxylic groups and the second peak can be assigned to the decomposition of the N-containing chemical moieties. The residual mass after the complete burning of the SER plant was near 0.8 wt.%.

In the case of SER sample loaded with Cu(II) ions (Cu-SER sample) in Fig. 4b, the peaks that are related to the carboxylic and N-containing surface groups are shifted on thermogravimetric diagram. The DTA peak related to carboxylic surface groups is shifted to 310°C and the peak associated with N-containing groups is moved to 413°C. This fact indicates the formation of chemical bonds between the Cu(II) ions and these moieties. Moreover, the additional small endothermic peak at 1009°C was detected. It can be suggested that this peak corresponds to the Cu2+ → Cu + reduction process or melting of metallic copper (Luiz and Nunes 2020). The residual mass after burning was near 5.9 wt.%. The similar situation is observed for Pb-SER sample (SER sample loaded with Pb(II) ions) in Fig. 4c. The peaks that are assigned to the carboxylic and N-containing surface groups are shifted on thermogravimetric diagram: for COOH groups from 324°C to 350°C and for N-containing groups from 480°C to 439°C. The mass of unburned residue was ~ 11 wt.%, that was much higher than obtained after complete burning of the raw SER plant adsorbent and twice as high as after the adsorption of Cu.

To shed more light on the functional groups potentially involved in the adsorption process, the FT-IR spectra of native SER adsorbent and the Cu-SER and Pb-SER samples were recorded (see Fig. 5). As can be seen, the stretching vibrations of hydroxyl surface groups in native SER plant ($\nu(\text{-OH})_{\text{bonded}}$ at 3322 cm^{-1}) are shifted to $\nu(\text{-OH})_{\text{bonded}}$ at 3290 cm^{-1} and 3274 cm^{-1} in Pb-SER and Cu-SER samples, respectively. The surface carboxylic groups possess their stretching vibrations at $\nu(\text{-C = O})$ = 1730 cm^{-1} and $\nu(\text{-C-O})$ = 1510 cm^{-1} in bare SER plant adsorbent. A shift to $\nu(\text{-C = O})$ = 1735 cm^{-1} and no shift for $\nu(\text{-C-O})$ = 1508 cm^{-1} in the Pb-SER sample confirms the participation of surface carboxylic groups in the elimination of Pb(II) ions. There is no shift in the stretching vibrations of $\nu(\text{-C = O})$ and $\nu(\text{-C-O})$ for Cu-SER sample which demonstrates the absence of interactions between these moieties and the Cu(II) ions. In the case of N-containing surface groups, the large shift in bending vibrations of aminogroups ($\delta(NH_2)$ = 1600cm^{-1}, 1629 cm^{-1} and 1614 cm^{-1} for SER adsorbent and Pb-SER and Cu-SER samples, respectively)

can be observed. The bending vibrations of hydroxyl surface groups in the native SER adsorbent δ(C-OH) at 1024 cm^{-1} can be related to plant polysaccharide components and are shifted during the adsorption: for Pb-SER sample δ(C-OH) = 1014 cm^{-1} and for Cu-SER sample δ(C-OH) = 1016 cm^{-1}. Therefore, this verifies the interactions between the hydroxyl moieties of plant components and the Pb(II) and Cu(II) ions. To sum up the observations from FT-IR, the interactions of carboxylic, hydroxyl and amino surface groups play an important role in the adsorptive removal of targeted heavy metals (Lu et al. 2012).

To investigate the surface chemistry of the pure SER and the corresponding metal-laden samples after the adsorption, XPS method was applied. Namely, the XPS spectra of C 1s,O 1s, Pb 4f and Cu 2p have been recorded (Fig. 6) and the changes of binding energies of target elements are shown in Table S2 in the Supplementary information.

The surface chemical composition of the SER biosorbent powder before and after the ionic adsorption was revealed by the XPS spectrum in Fig. 6a, where the carbon-based compounds of the organic SER plant and the adsorbed Cu and Pb peaks are present in the corresponding loaded samples. The bare SER plant showed the presence of impurities such as fluorine and silicon, which were washed out after the adsorption experiments. Despite the presence of the mentioned impurities, the SER biosorbent plant revealed its organic nature by the characteristic C 1s and O 1s peaks in Fig. 6b and Fig. 6c, respectively.

The core-level spectra decomposition of the C 1s (Fig. 6b) for pure SER plant was fitted in 4 main peaks positioned at 284.7 eV, 286.4 eV, 287.9 eV, and 288.9 eV, which are generally assigned to C-C, organic -C-O-, -C = O, and -C-F/COO species, respectively (Smith et al. 2016). Similarly, C 1s spectra of the SER biosorbent after the Cu and Pb adsorption was decomposed into 4 peaks, which binding energies were close to the ones detected for the pure plant. Interestingly, the peak attributed to the -C-O- group increased its intensity at the binding energy of 286.2 eV.

The decomposition of the O 1s spectrum (Fig. 6c) suggested that for pure SER biosorbent the presence of oxygen is only attributed to organic C-O or C = O compounds (binding energy, BE = 532.5 eV) (Smith et al. 2016; Wang et al. 2017). After the adsorption, the O 1s core-level spectra of both Cu-SER and Pb-SER samples were broadened by lateral bumps with deconvoluted peaks around 531.2 eV and 533.7 eV, which are assigned to metal carbonates or oxides and alcohol groups, respectively (Wang et al. 2017).

The analysis of the Pb 4f (Fig. 6d) spectrum revealed the presence of the characteristic doublet with the $4f_{7/2}$ and $4f_{5/2}$ spin-orbital levels distanced by 4.8 eV, suggesting the presence of Pb(II) species, which, after analysing the O 1s peak, can be connected to oxidized compounds such as $Pb(OH)_2$ or PbO (Taylor and Perry 1984; Rondon and Sherwood 1998). However, it is difficult to determine the nature of the adsorbed lead substances, as almost all oxygen-containing lead compounds have a peak in this BE range (Laajalehto et al. 1993).

In the case of Cu adsorption, the characteristic doublet of the Cu 2p core-level spectrum (Fig. 6d) presented the spin-orbital levels positioned at 933.3 eV and 953.2 eV, attributed to the Cu $2p_{3/2}$ and Cu

$2p_{1/2}$ spin orbitals with a ΔBE of 19.9 eV. The presence of weak intensity satellite features between 938 and 946 eV suggests the presence of Cu(I) species, such as Cu_2O, rather than Cu(II) compounds (Biesinger 2017; Li et al. 2018; Liu et al. 2019b).

The changes of pH that occurred at each point of Cu(II) and Pb(II) adsorption isotherms are illustrated in Fig. 7. The calculation was done by subtracting the final pH after adsorption from the pH of the starting solution at the beginning of the adsorption (pH_s-pH_f). As demonstrated, both curves have negative and positive ranges. At the beginning of the adsorption isotherms (namely, at low concentrations of target ions), the changes of pH are negative, meaning that pH_s is lower than pH_f. This can be explained by the release of alkali and alkaline earth metals (see Table S3 in Supplementary information) that increased the pH. This release is related to the ion exchange mechanism of total adsorption process (Cui et al. 2016). Other parts of the curves showed the positive changes of pH, implying that pH_s is higher than pH_f. This can be interpreted as the release of additional hydrogen cations from the reactive carboxylic, amino and hydroxyl groups on the SER surface. It can be concluded that at higher Cu(II) and Pb(II) concentrations, the complexation and chelation are involved in the adsorption. Therefore, the adsorption of target metals consists of the ion exchange at the lower Cu(II) and Pb(II) concentrations and the complexation and chelation at the higher contaminants' concentrations.

The measurements of ζ-potential for the bare SER plant and the samples Cu-SER and Pb-SER after adsorption showed the decrease of the negative charge after the adsorption processes (Table 3). This can be explained by the binding of negatively charged surface groups (mainly carboxylic) with metal ions.

Table 3
The ζ-potential and pH values changes of the point of zero charge of the native SER plant and samples after adsorption

Sample	ζ-potential	pH
SER	-25.4	5.9
Pb-SER	-18.1	5.2
Cu-SER	-18.1	5.2

4. Conclusions

The proposed research work was dealing with the adsorption of Cu(II) and Pb(II) ions on the eco-friendly plant biosorbent- *Thymus serpyllum* L. (wild thyme). The best adsorption parameters for both ions in terms of pH, contact time and adsorbent dosage were established. Good adsorption ability was evidenced despite the fact that the plant was used in its native state (no biochar was produced). The combined adsorption in the binary metal system showed very high removal efficiency for Pb(II) ions

(90.1%). The adsorption kinetics was found to be very rapid and followed the pseudo-second-order model with the correlation coefficients 0.9997 and 0.9961 for Cu(II) and Pb(II) ions, respectively. According to the isotherm modelling, the Langmuir model described the adsorption of Cu(II) ions better, which implied that the adsorption of Cu(II) ions was limited to one molecular layer. The adsorption of Pb(II) ions was better defined by the Freundlich isotherm model, which suggested that the adsorption occurred on the heterogeneous surface of the biosorbent. The highest experimentally obtained adsorption capacity was 12.66 mg g^{-1} after 10 minutes of adsorption at 16 g L^{-1} adsorbent dosage for Cu(II) ions and 53.13 mg g^{-1} after 30 minutes of adsorption at 12 g L^{-1} adsorbent dosage for Pb(II) ions. The biosorbent was characterized by the combination of various methods including SEM/EDX, TGA, FT-IR, XPS and measurement of ζ-potential. The TGA and FT-IR results revealed that the hydroxyl and amino surface groups played an important role during the adsorption of both metal ions and for Pb(II) ions also the carboxylic groups were involved. The XPS analysis of the samples after adsorption revealed that Cu(II) ions were adsorbed in the form of Cu(I) species (most probably Cu_2O) and Pb(II) ions as oxidized compounds such as $Pb(OH)_2$ or PbO. The determination of the adsorption mechanism showed the complexity of the adsorption process consisting of the ion exchange at lower Cu(II) and Pb(II) concentrations and the complexation and chelation at higher concentrations of targeted heavy metals.

Declarations

Funding

The study was supported by the Slovak Agency for Science and Development (project no. APVV-18-0357) and by the Slovak Grant Agency VEGA (project no. 2/0112/22). Part of the work was carried out on the devices purchased by CEITEC Nano Research Infrastructure supported by MEYS-CR (LM2018110).

Competing Interests

The authors have no relevant financial or non-financial interests to disclose.

Ethical Approval

Not applicable

Consent to Participate

Not applicable

Consent to Publish

Not applicable

Availability of data and materials

The data and materials are available upon electronic communication with the authors.

Authors contributions

All authors contributed to the study conception and design. Material preparation, data collection and analysis were performed by Mária Kováčová, Halyna Yankovych, Mariano Casas-Luna, Michaela Remešová, Lenka Findoráková, Martin Stahorský and Matej Baláž. Matej Baláž and Ladislav Čelko supervised the studies and provided the financial support from their projects. The first draft of the manuscript was written by Mária Kováčová and all authors commented on previous versions of the manuscript. All authors read and approved the final manuscript.

References

1. Adriano DC (2001) Trace Elements in Terrestrial Environments: Biogeochemistry, Bioavailability, and Risks of Metals. Springer, New York, NY, New York
2. Awual MR, Yaita T, El-Safty SA et al (2013) Copper(II) ions capturing from water using ligand modified a new type mesoporous adsorbent. Chem Eng J 221:322–330. https://doi.org/10.1016/j.cej.2013.02.016
3. Baláž M (2021) Environmental Mechanochemistry: Recycling Waste into Materials using High-Energy Ball Milling. Springer Nature, Cham
4. Bayo J (2012) Kinetic studies for Cd(II) biosorption from treated urban effluents by native grapefruit biomass (Citrus paradisi L.): The competitive effect of Pb(II), Cu(II) and Ni(II). Chem Eng J 191:278–287. https://doi.org/10.1016/j.cej.2012.03.016
5. Beni AA, Esmaeili A (2020) Biosorption, an efficient method for removing heavy metals from industrial effluents: A Review. Environ Technol Innov 17. https://doi.org/10.1016/j.eti.2019.100503. ARTN 100503
6. Bhattacharyya KG, Sen Gupta S (2006) Adsorption of Fe(III) from water by natural and acid activated clays: Studies on equilibrium isotherm, kinetics and thermodynamics of interactions. Adsorption-Journal of the International Adsorption Society 12:185–204. https://doi.org/10.1007/s10450-006-0145-0
7. Biesinger MC (2017) Advanced analysis of copper X-ray photoelectron spectra. Surf Interface Anal 49:1325–1334. https://doi.org/10.1002/sia.6239
8. Cruz-Olivares J, Perez-Alonso C, Barrera-Diaz C et al (2010) Inside the removal of lead(II) from aqueous solutions by De-Oiled Allspice Husk in batch and continuous processes. J Hazard Mater 181:1095–1101. https://doi.org/10.1016/j.jhazmat.2010.05.127
9. Cui SH, Zhang R, Peng YT et al (2021) New insights into ball milling effects on MgAl-LDHs exfoliation on biochar support: A case study for cadmium adsorption. J Hazard Mater 416:11. https://doi.org/10.1016/j.jhazmat.2021.126258
10. Cui XQ, Fang SY, Yao YQ et al (2016) Potential mechanisms of cadmium removal from aqueous solution by Canna indica derived biochar. Sci Total Environ 562:517–525. https://doi.org/10.1016/j.scitotenv.2016.03.248

11. Czikkely M, Neubauer E, Fekete I et al (2018) Review of Heavy Metal Adsorption Processes by Several Organic Matters from Wastewaters. Water 10: ARTN 1377. https://doi.org/10.3390/w10101377
12. Duan CT, Zhao N, Yu XL et al (2013) Chemically modified kapok fiber for fast adsorption of Pb^{2+}, Cd^{2+}, Cu^{2+} from aqueous solution. Cellulose 20:849–860. https://doi.org/10.1007/s10570-013-9875-9
13. Elangovan R, Philip L, Chandraraj K (2008) Biosorption of hexavalent and trivalent chromium by palm flower (Borassus aethiopum). Chem Eng J 141:99–111. https://doi.org/10.1016/j.cej.2007.10.026
14. European Parliament and Council of the European Union (2020) Directive (EU) 2020/2184 of the European Parliament and of the Council of 16 December 2020 on the quality of water intended for human consumption. Official J Eur Union L 435:1–62
15. Forgionny A, Acelas NY, Ocampo-Perez R et al (2021) Understanding mechanisms in the adsorption of lead and copper ions on chili seed waste in single and multicomponent systems: a combined experimental and computational study. Environ Sci Pollut Res 28:23204–23219. https://doi.org/10.1007/s11356-020-11721-z
16. Freundlich HMF (1906) Over the adsorption in solution. J Phys Chem 57:385–470
17. Guerrero-Jimenez M, Calahorro C, Rojas LG (2019) Wilson disease and psychiatric symptoms: A brief case report. Gen Psychiatry 32:4. https://doi.org/10.1136/gpsych-2019-100066
18. Ho YS, Wase DAJ, Forster CF (1996) Kinetic studies of competitive heavy metal adsorption by Sphagnum moss peat. Environ Technol 17:71–77. https://doi.org/10.1080/09593331708616362
19. Huang XX, Liu YG, Liu SB et al (2016) Effective removal of Cr(VI) using beta-cyclodextrin-chitosan modified biochars with adsorption/reduction bifuctional roles. RSC Adv 6:94–104. https://doi.org/10.1039/c5ra22886g
20. Huang YH, Hsueh CL, Huang CP et al (2007) Adsorption thermodynamic and kinetic studies of Pb(II) removal from water onto a versatile Al_2O_3-supported iron oxide. Sep Purif Technol 55:23–29. https://doi.org/10.1016/j.seppur.2006.10.023
21. Chen JY, Sun LF, Negulescu II et al (2017) Fabrication and evaluation of regenerated cellulose/nanoparticle fibers from lignocellulosic biomass. Biomass & Bioenergy 101:1–8. https://doi.org/10.1016/j.biombioe.2017.03.024
22. Ibrahim D, Froberg B, Wolf A et al (2006) Heavy metal poisoning: Clinical presentations and pathophysiology. Clin Lab Med 26:67–97. https://doi.org/10.1016/j.cll.2006.02.003
23. Jovanovic AA, Dordevic VB, Zdunic GM et al (2017) Optimization of the extraction process of polyphenols from Thymus serpyllum L. herb using maceration, heat- and ultrasound-assisted techniques. Sep Purif Technol 179:369–380. https://doi.org/10.1016/j.seppur.2017.01.055
24. Kong ZL, Li XC, Tian JY et al (2014) Comparative study on the adsorption capacity of raw and modified litchi pericarp for removing Cu(II) from solutions. J Environ Manage 134:109–116. https://doi.org/10.1016/j.jenvman.2014.01.007

25. Laajalehto K, Smart RS, Ralston J et al (1993) STM and XPS investigation of reaction of galena in air. Appl Surf Sci 64:29–39. https://doi.org/10.1016/0169-4332(93)90019-8
26. Lagergren S (1898) About the Theory of so Called Adsorption of Soluble Substances (Zur Theorie der sogenannten Adsorption gelöster Stoffe). Kungliga Svenska Vetenskapsakademiens Handlingar 24:1–39
27. Langmuir I (1916) The constitution and fundamental properties of solids and liquids Part I Solids. JACS 38:2221–2295. https://doi.org/10.1021/ja02268a002
28. Li D, Wang GN, Cheng LM et al (2018) Engineering the Self-Assembly Induced Emission of Copper Nanoclusters as 3D Nanomaterials with Mesoporous Sphere Structures by the Crosslinking of Ce^{3+}. Acs Omega 3:14755–14765. https://doi.org/10.1021/acsomega.8b02204
29. Littera P, Urik M, Sevc J et al (2011) The potential of *Thymus serpyllum* biomass for removal of antimony(III) from aqueous environment. Fresenius Environ Bull 20:2959–2963
30. Liu LL, Luo XB, Ding L et al (2019a) Application of nanotechnology in the removal of heavy metal from water. Elsevier Science Bv, Amsterdam
31. Liu R, Zuo L, Huang XR et al (2019b) Colorimetric determination of lead(II) or mercury(II) based on target induced switching of the enzyme-like activity of metallothionein-stabilized copper nanoclusters. Microchim Acta 186: ARTN 250. https://doi.org/10.1007/s00604-019-3360-6
32. Lu HL, Zhang WH, Yang YX et al (2012) Relative distribution of Pb^{2+} sorption mechanisms by sludge-derived biochar. Water Res 46:854–862. https://doi.org/10.1016/j.watres.2011.11.058
33. Luiz JM, Nunes RS (2020) Synthesis, characterization, and thermal behavior of amidosulfonates of transition metals in air and nitrogen atmosphere. Eclética Química 45:32–39. https://doi.org/10.26850/1678-4618eqj.v45.4.2020.p32-39
34. Mahaninia MH, Rahimian P, Kaghazchi T (2015) Modified activated carbons with amino groups and their copper adsorption properties in aqueous solution. Chin J Chem Eng 23:50–56. https://doi.org/10.1016/j.cjche.2014.11.004
35. Martinez M, Miralles N, Hidalgo S et al (2006) Removal of lead(II) and cadmium(II) from aqueous solutions using grape stalk waste. J Hazard Mater 133:203–211. https://doi.org/10.1016/j.jhazmat.2005.10.030
36. Moore MR (1988) Haematological effects of lead. Sci Total Environ 71:419–431. https://doi.org/10.1016/0048-9697(88)90214-8
37. Mudhoo A, Garg VK, Wang SB (2012) Removal of heavy metals by biosorption. Environ Chem Lett 10:109–117. https://doi.org/10.1007/s10311-011-0342-2
38. Oliveira WE, Franca AS, Oliveira LS et al (2008) Untreated coffee husks as biosorbents for the removal of heavy metals from aqueous solutions. J Hazard Mater 152:1073–1081. https://doi.org/10.1016/j.jhazmat.2007.07.085
39. Reddy DHK, Ramana DKV, Seshaiah K et al (2011) Biosorption of Ni(II) from aqueous phase by Moringa oleifera bark, a low cost biosorbent. Desalination 268:150–157.

https://doi.org/10.1016/j.desal.2010.10.011

40. Rondon S, Sherwood PMA (1998) Core Level and Valence Band Spectra of PbO by XPS. Surf Sci Spectra 5:97–103. https://doi.org/10.1116/1.1247866
41. Sert S, Kutahyali C, Inan S et al (2008) Biosorption of lanthanum and cerium from aqueous solutions by Platanus orientalis leaf powder. Hydrometallurgy 90:13–18. https://doi.org/10.1016/j.hydromet.2007.09.006
42. Shafeeyan MS, Daud W, Houshmand A et al (2010) A review on surface modification of activated carbon for carbon dioxide adsorption. J Anal Appl Pyrolysis 89:143–151. https://doi.org/10.1016/j.jaap.2010.07.006
43. Schmuhl R, Krieg HM, Keizer K (2001) Adsorption of Cu(II) and Cr(VI) ions by chitosan: Kinetics and equilibrium studies. Water Sa 27:1–7. https://doi.org/10.4314/wsa.v27i1.5002
44. Smith M, Scudiero L, Espinal J et al (2016) Improving the deconvolution and interpretation of XPS spectra from chars by ab initio calculations. Carbon 110:155–171. https://doi.org/10.1016/j.carbon.2016.09.012
45. Taylor JA, Perry DL (1984) An x-ray photoelectron and electron energy loss study of the oxidation of lead. J Vacuum Sci Technol A 2:771–774. https://doi.org/10.1116/1.572569
46. Ucer A, Uyanik A, Aygun SF (2006) Adsorption of Cu(II), Cd(II), Zn(II), Mn(II) and Fe(III) ions by tannic acid immobilised activated carbon. Sep Purif Technol 47:113–118. https://doi.org/10.1016/j.seppur.2005.06.012
47. Wan MW, Kan CC, Rogel BD et al (2010) Adsorption of copper (II) and lead (II) ions from aqueous solution on chitosan-coated sand. Carbohydr Polym 80:891–899. https://doi.org/10.1016/j.carbpol.2009.12.048
48. Wang J, Liu TL, Huang QX et al (2017) Production and characterization of high quality activated carbon from oily sludge. Fuel Process Technol 162: 13–19. https://doi.org/10.1016/j.fuproc.2017.03.017
49. Witek-Krowiak A (2012) Analysis of temperature-dependent biosorption of Cu^{2+} ions on sunflower hulls: Kinetics, equilibrium and mechanism of the process. Chem Eng J 192:13–20. https://doi.org/10.1016/j.cej.2012.03.075
50. Witek-Krowiak A, Szafran RG, Modelski S (2011) Biosorption of heavy metals from aqueous solutions onto peanut shell as a low-cost biosorbent. Desalination 265:126–134. https://doi.org/10.1016/j.desal.2010.07.042
51. Xu L, Liu YN, Wang JG et al (2021) Selective adsorption of Pb^{2+} and Cu^{2+} on amino-modified attapulgite: Kinetic, thermal dynamic and DFT studies. J Hazard Mater 404:10. https://doi.org/10.1016/j.jhazmat.2020.124140
52. Yankovych H, Novoseltseva V, Kovalenko O et al (2021) New perception of Zn(II) and Mn(II) removal mechanism on sustainable sunflower biochar from alkaline batteries contaminated water. J Environ Manage 292: ARTN 112757. https://doi.org/10.1016/j.jenvman.2021.112757

53. Zou ZM, Tang YL, Jiang CH et al (2015) Efficient adsorption of Cr(VI) on sunflower seed hull derived porous carbon. J Environ Chem Eng 3:898–905. https://doi.org/10.1016/j.jece.2015.02.025

Figures

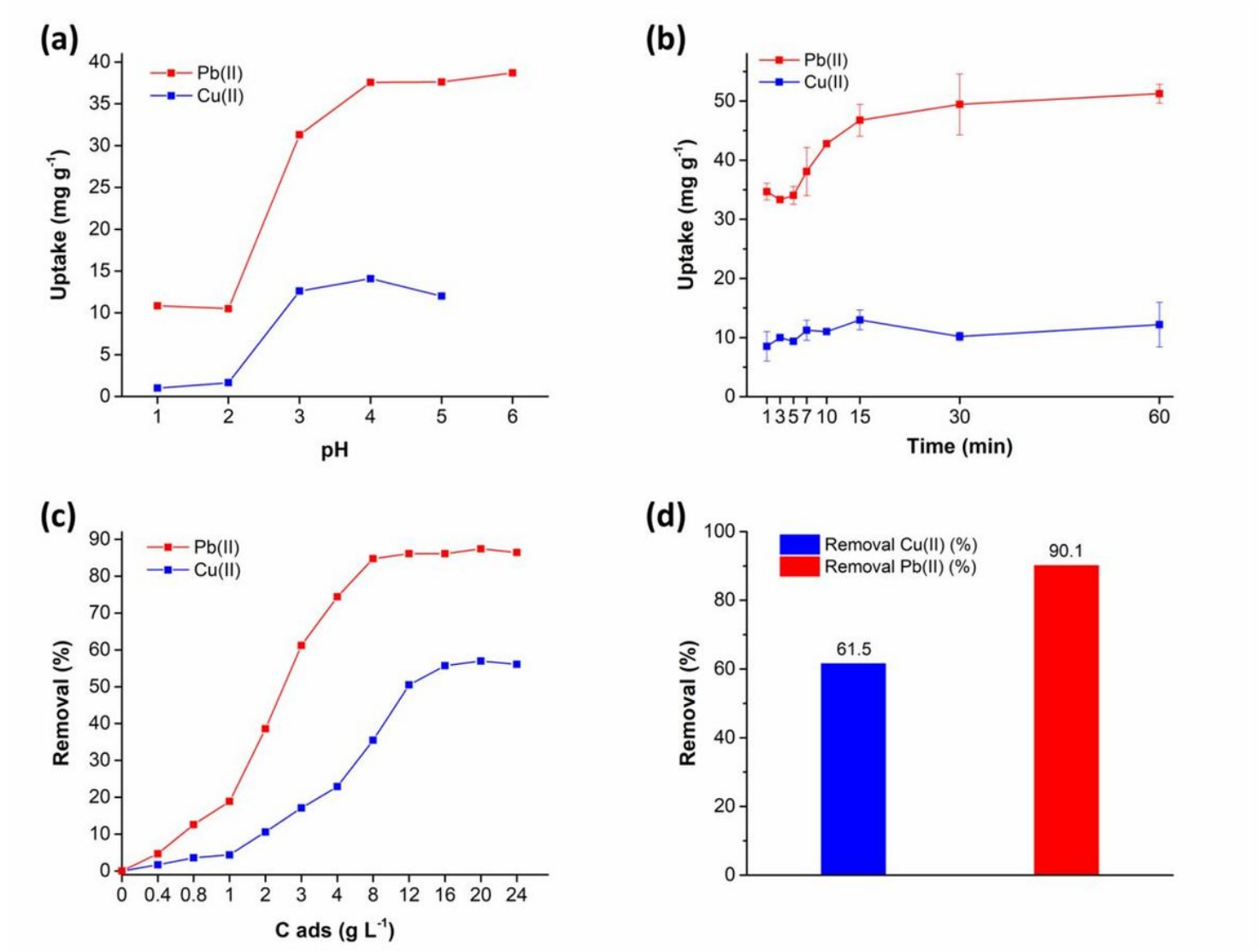

Figure 1

Effect of the different variables on the adsorption of Cu(II) and Pb(II) ions onto *Thymus serpyllum* biosorbent: (a) pH; (b) contact time; (c) adsorbent dosageô (d) binary metal solution

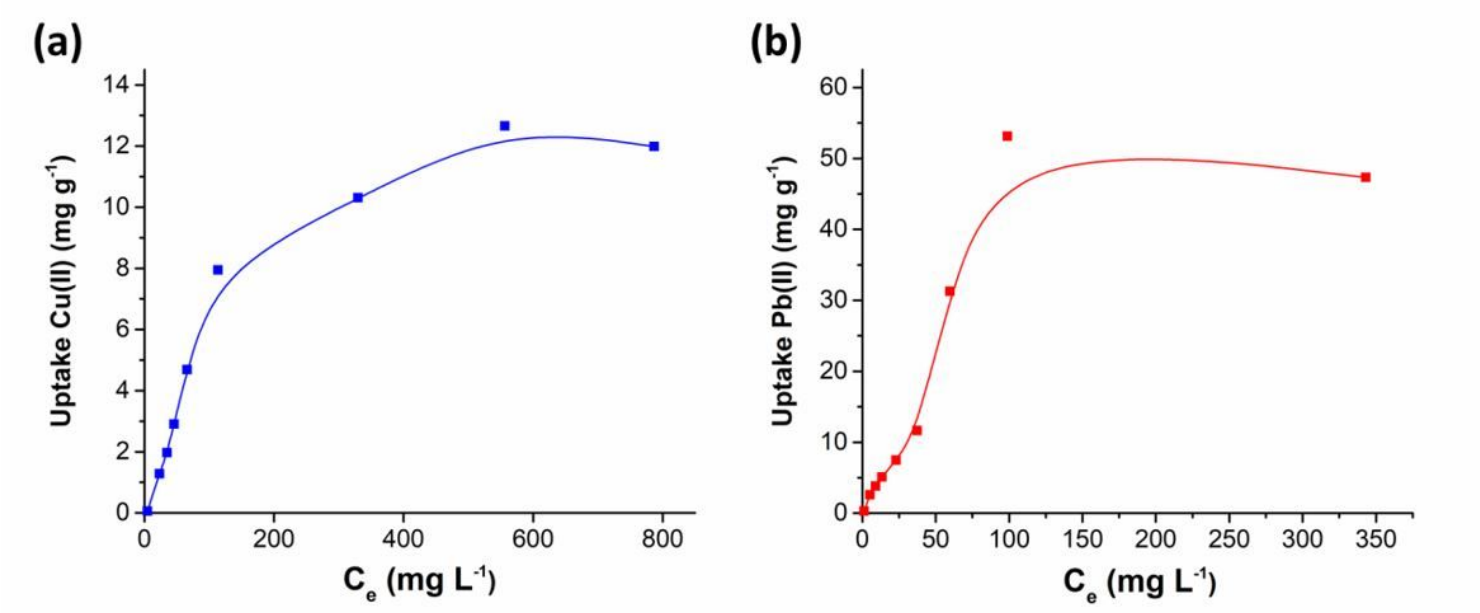

Figure 2

The adsorption isotherms for the adsorption of (a) Cu(II) and (b) Pb(II) ions

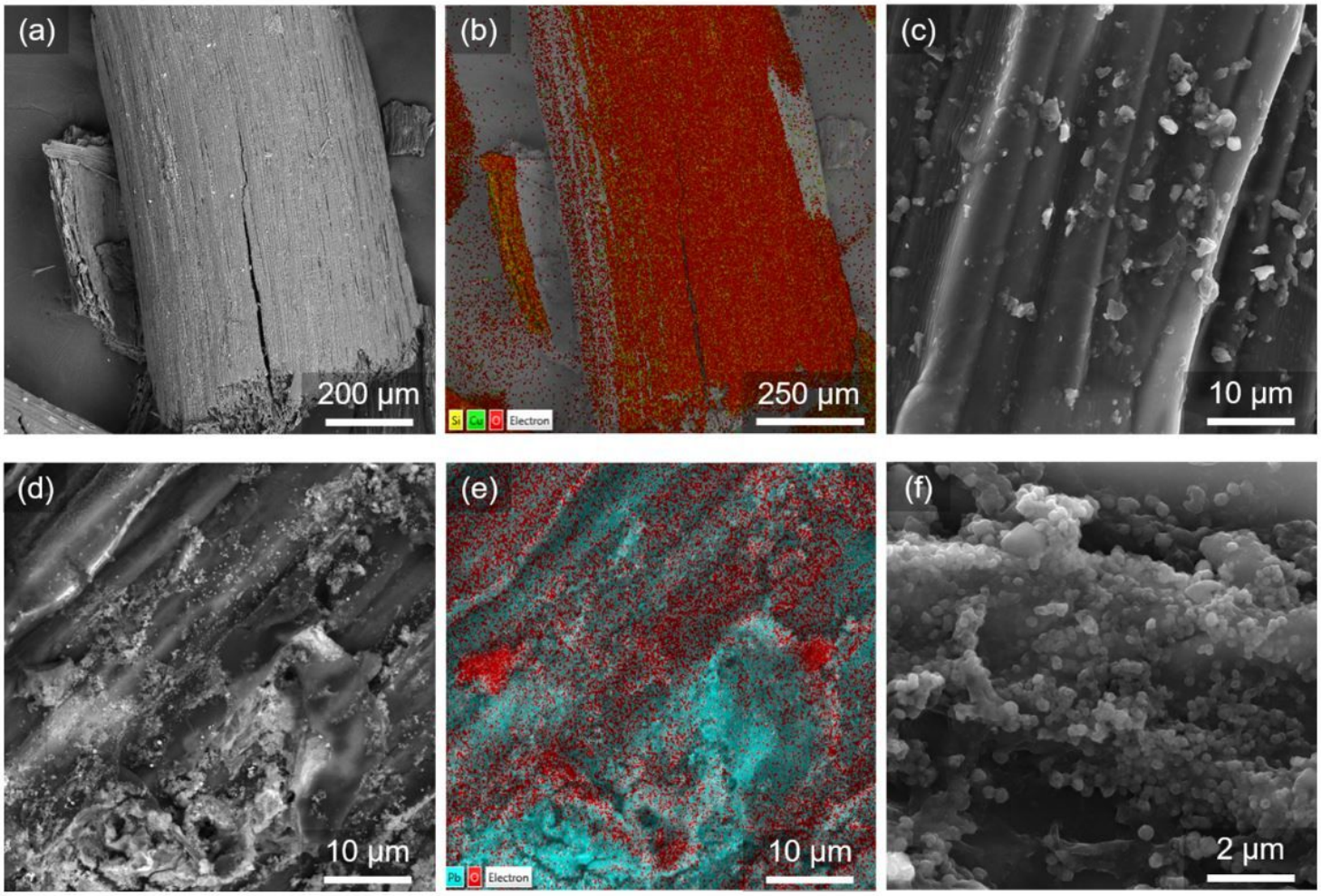

Figure 3

SEM micrographs and EDX mapping of *Thymus serpyllum* biosorbent surface after the adsorption of (a-c) Cu(II) and (d-f) Pb(II) ions; (a, d) surface morphology overview (SEM-BSE); (b, e) EDX layered map, (c, f) surface detail (SEM-SE)

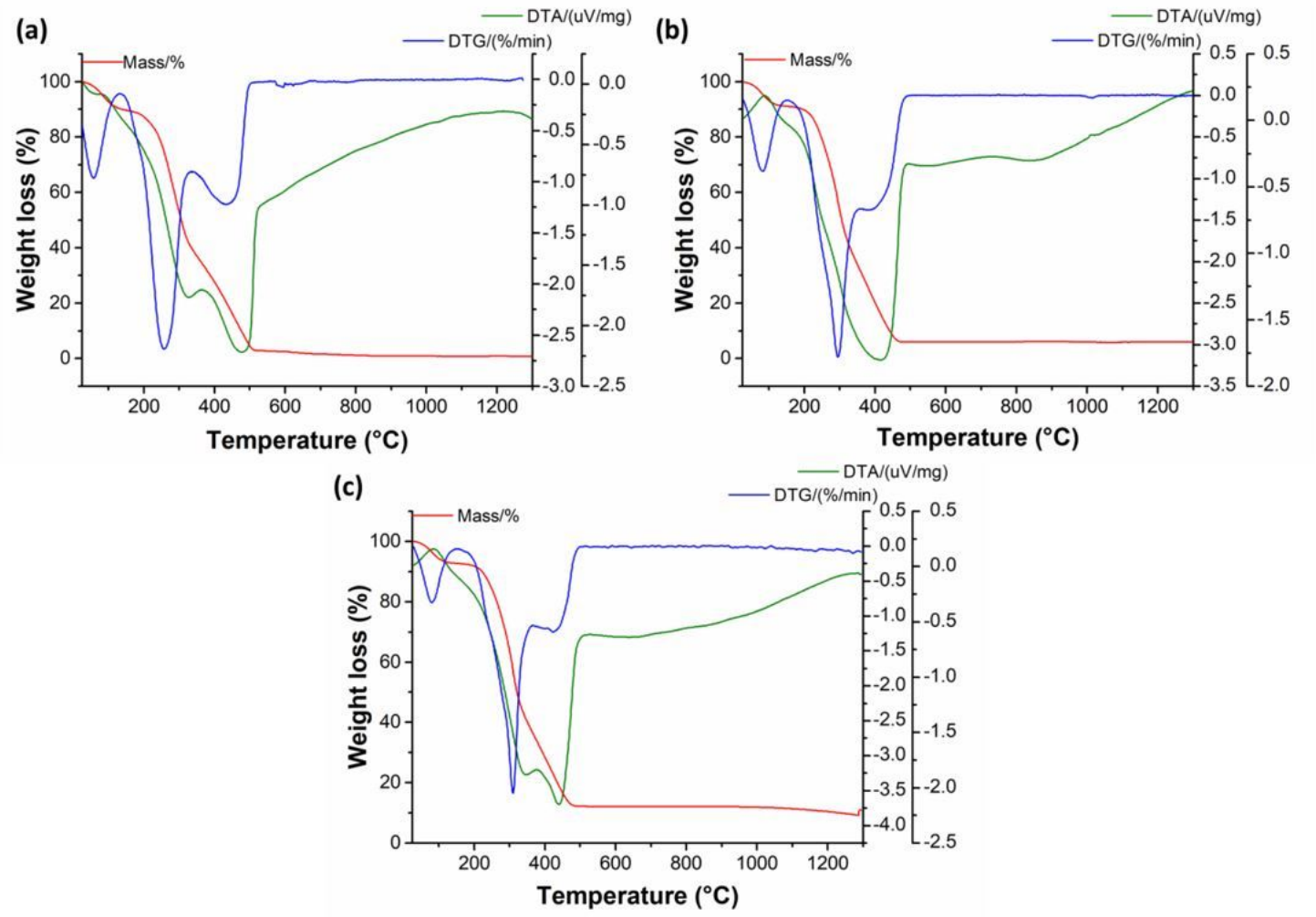

Figure 4

TG/DTG and DTA curves of (a) native *Thymus serpyllum* biosorbent and *Thymus serpyllum* biosorbent loaded with (b) Cu(II) and (c) Pb(II) ions after adsorption

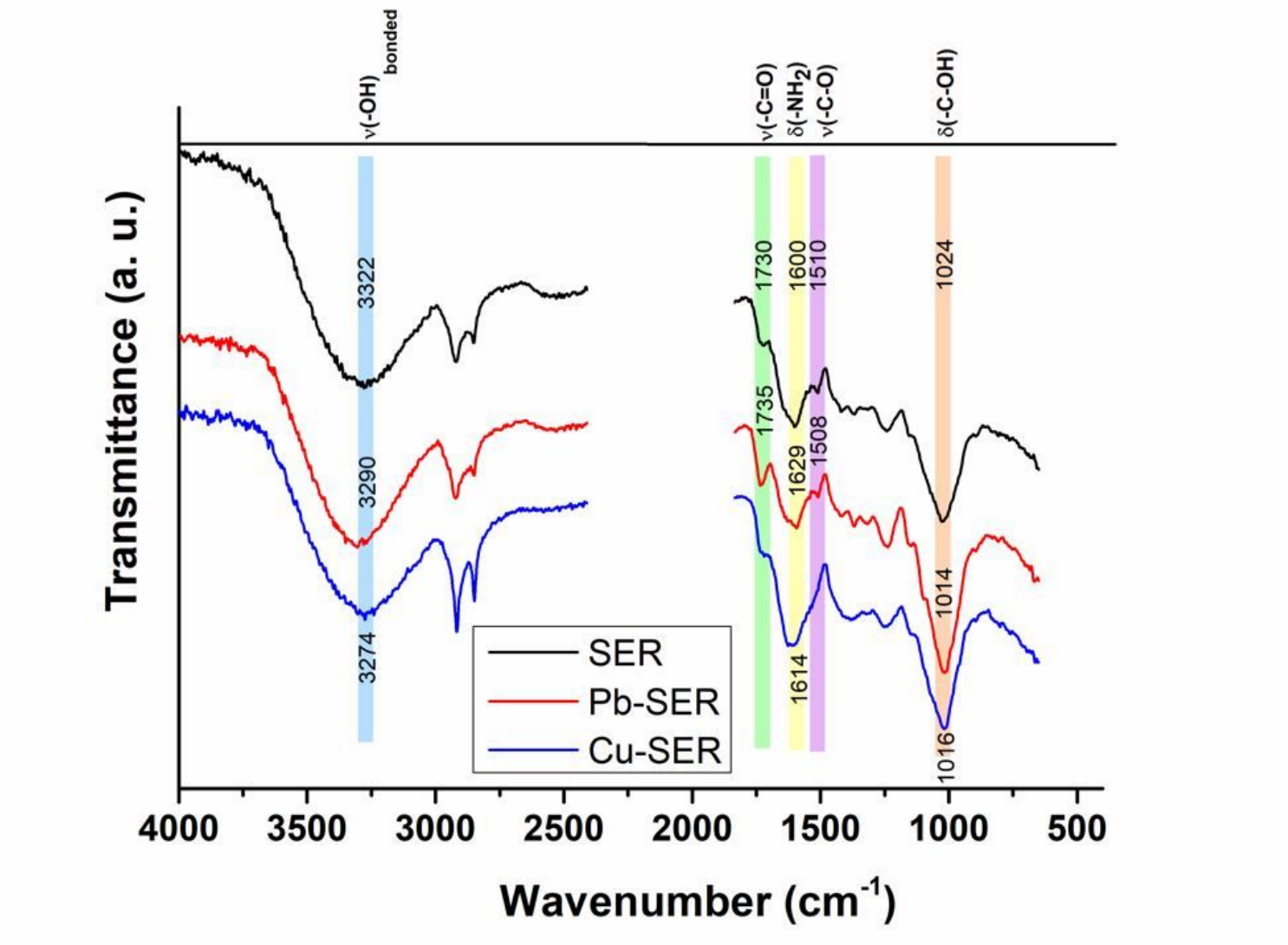

Figure 5

The FT-IR spectra of native *Thymus serpyllum* biosorbent and the samples after the adsorption of Pb(II) (Pb-SER) and Cu(II) (Cu-SER) ions

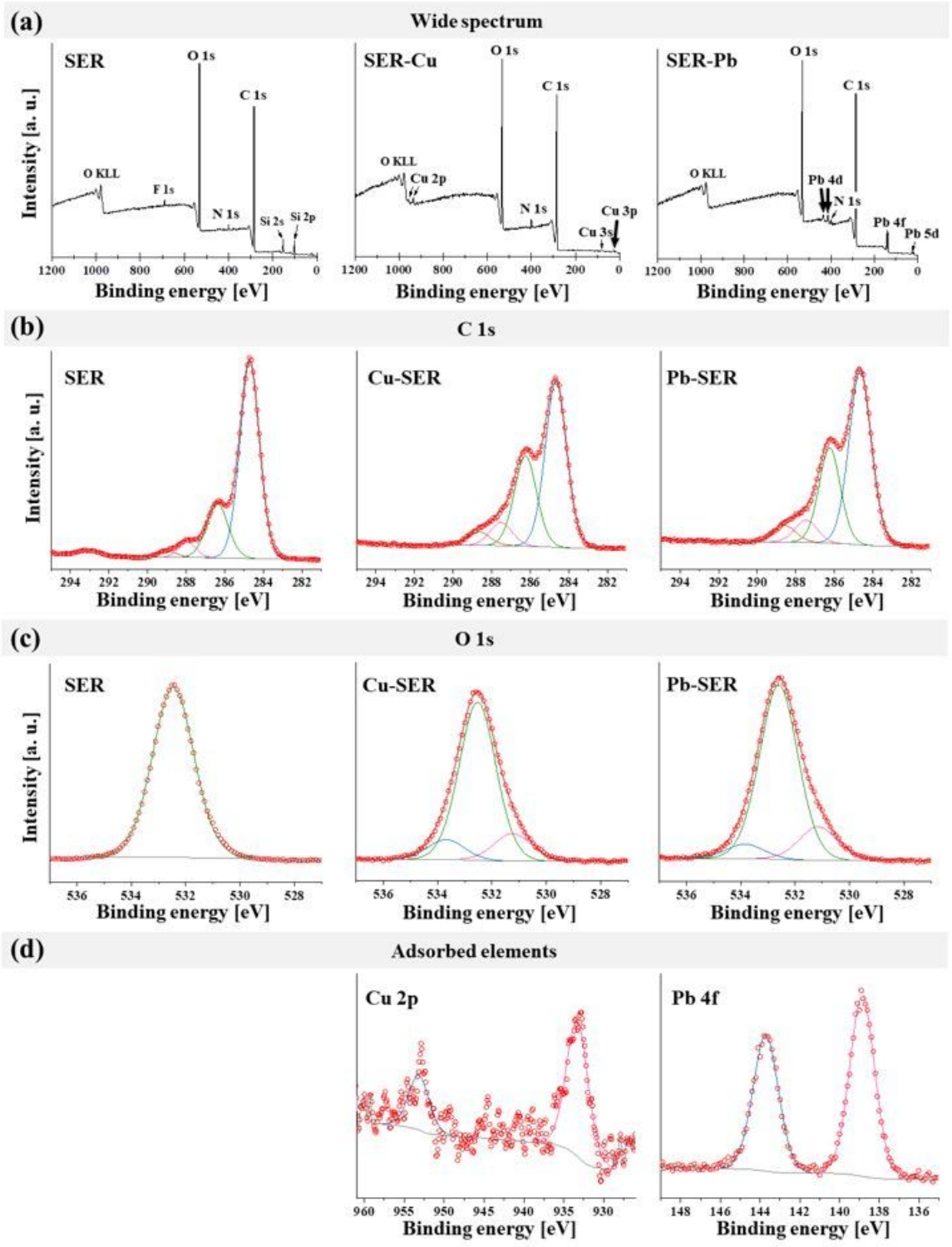

Figure 6

XPS spectra of pure SER biosorbent before and after Cu and Pb adsorption. a) survey spectra; b) high-resolution spectra and deconvolution of C 1s peak; c) high-resolution spectra and deconvolution of O 1s peak; and d) high-resolution spectra and deconvolution of the adsorbed Cu and Pb elements for the Cu 2p and Pb 4f peaks, respectively

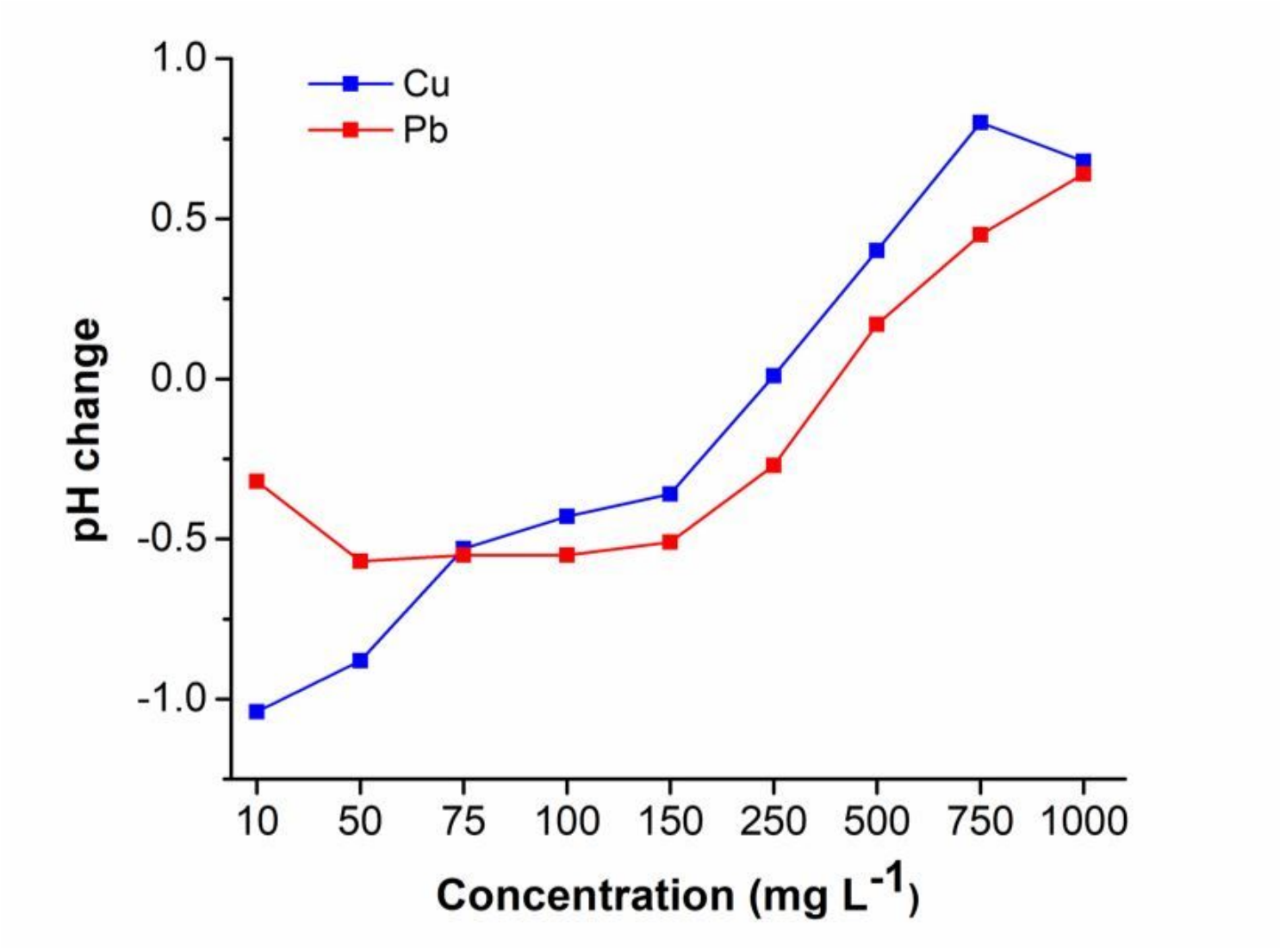

Figure 7

The changes of pH during the adsorption of Cu(II) and Pb(II) ions

Supplementary Files

This is a list of supplementary files associated with this preprint. Click to download.

- GAManuscriptadsorption.jpg
- renamed01a8f.docx